Charge-exchange reactions accompanied by a single π^+ production in medium-energy heavy-ion collisions*

Xiaolei Chen (陈晓磊)[1,2†] Jinyu Yang (杨谨渝)[1,2‡] Shikang Dong (董世康)[1,2§] Baowei Ding (丁宝卫)[1,2♮] Bitao Hu (胡碧涛)[1,2♯] Xiyu Qiu (邱玺玉)[1,2¶]

[1]Frontiers Science Center for Rare Isotopes, Lanzhou University, Lanzhou 730000, China
[2]School of Nuclear Science and Technology, Lanzhou University, Lanzhou 730000, China

Abstract: Heavy-ion charge-exchange (CE) reactions provide a sensitive probe of isospin dynamics in nuclear collisions. We investigate the reaction $^{12}C(^{12}C, {}^{12}N\pi^+)^{12}Be$ at 400−600 A MeV using the ultra-relativistic quantum molecular dynamics model coupled with a phase-space coalescence approach. This reaction constitutes a nontrivial CE channel accompanied by single π^+ production in heavy-ion collisions, thereby extending previous studies from lepton-induced to hadronic systems. The ^{12}N fragment is formed via nucleon and meson exchange, while π^+ production is primarily governed by Δ resonance excitation and decay; this dual mechanism enables the simultaneous investigation of CE processes and Δ-induced pion production within the same reaction system. We calculate the reaction cross section and analyze the four-momentum distributions of ^{12}N and π^+. Characteristic phase-space features reflect these distinct production mechanisms and offer guidance for future experimental design. Furthermore, this reaction could serve as a pathway for rare-isotope production.

Keywords: heavy-ion charge-exchange reaction, π^+ production, Δ resonance, UrQMD model, phase-space coalescence

DOI: 10.1088/1674-1137/ae9050 **CSTR:** 32044.14.ChinesePhysicsC.50114101

I. INTRODUCTION

Heavy-ion collisions provide a powerful platform for studying strong interactions and the properties of nuclear matter. By spanning a wide range of incident energies, these collisions probe nuclear matter under diverse conditions, ranging from sub-saturation densities to extremely high-temperature and high-density environments. At low and intermediate energies, heavy-ion reactions provide important insights into nuclear reaction mechanisms, the nuclear matter equation of state (EoS), and the evolution of nuclear shell structure [1−9]. At higher energies, they enable the formation of hot and dense hadronic matter and may lead to the creation of a quark–gluon plasma (QGP) [10−14], offering insights into the state of matter in the early universe shortly after the Big Bang. Furthermore, high-energy collisions can produce various strange particles and hypernuclei [15−18]. Studies of hypernuclei place constraints on hyperon–nucleon (Y–N) and hyperon–hyperon (Y–Y) interactions and are essential for understanding neutron stars [17, 19−22].

Among the various reactions in heavy-ion physics, charge-exchange (CE) reactions play a unique role. These reactions are characterized by the transfer of charge between the projectile and target while conserving the mass number. At low energies, CE reactions are dominated by proton–neutron exchange mechanisms between nucleons [23]. As collision energy increases, charged-meson exchange processes become increasingly important and compete with nucleon exchange [24]. Because protons and neutrons represent two isospin states of the nucleon, CE reactions can be interpreted as isospin transitions induced by the strong interaction. Such processes are analogous to nuclear β decay and thus serve as an effective probe of β-like transitions [25]. Consequently, CE reactions offer access to nuclear matrix elements (NMEs) relevant to weak-interaction processes, including neutrino–nucleus reactions and neutrinoless double-β decay

Received 9 February 2026; Accepted 24 July 2026; Accepted manuscript online 25 July 2026

* This work was supported by the National Key Research and Development Program of China (2022YFE0103900) and the Fundamental Research Funds for the Central Universities (lzujbky-2023-stlt01)

† E-mail: xiaoleichen15@gmail.com
‡ E-mail: 1799512527@qq.com
§ E-mail: dongshk2025@lzu.edu.cn
♮ E-mail: dingbw@lzu.edu.cn
♯ E-mail: hubt@lzu.edu.cn
¶ E-mail: qiuxy@lzu.edu.cn

($0\nu\beta\beta$) [26, 27]. Furthermore, CE studies contribute to a deeper understanding of meson-exchange mechanisms, nucleon–nucleon correlations, and spin–isospin excitations in nuclei [28−31].

Medium- and high-energy heavy-ion CE reactions also provide potential pathways for producing hypernuclei, particularly neutron-rich and neutral hypernuclei [32], such as ${}^{2}_{\Lambda}$n, ${}^{3}_{\Lambda}$n, ${}^{6}_{\Lambda}$H, and ${}^{7}_{\Lambda}$H. Investigations of these systems address fundamental questions regarding the possible existence of neutral hypernuclei and the origin of the extremely short lifetimes observed in neutron-rich hypernuclei [33]. However, owing to their extremely small production cross sections and the scarcity of experimental data—particularly at high energies—these studies remain largely theoretical; thus, further experimental verification is required.

Among various reaction mechanisms, experimental studies have shown that reactions involving Δ^+ excitation can produce rare isotopes of interest, wherein the Δ^+ resonance decays via π^+ and neutron emission [34]. Although these processes are typically induced by leptons, the underlying mechanism is universal and equally applicable to heavy-ion collisions.

In this paper, we present a systematic theoretical investigation of the ^{12}C(^{12}C, ^{12}Nπ^+)^{12}Be reaction using the ultra-relativistic quantum molecular dynamics (UrQMD) model. This reaction represents a nontrivial heavy-ion charge-exchange (CE) channel accompanied by single π^+ production. Compared with conventional CE studies focusing on nucleon-induced or light-ion reactions, this work extends the investigation to a heavy-ion system, thereby providing a new perspective on isospin dynamics and meson production in a many-body environment. A distinctive feature of this reaction is that both CE processes and Δ resonance excitation and decay occur within the same system, enabling the study of these mechanisms under identical reaction conditions.

Using the UrQMD model, we calculate the reaction cross section and systematically analyze the four-momentum distributions of the emitted ^{12}N and π^+ particles. Multidimensional distributions in momentum, energy, emission angle, and rapidity exhibit characteristic phase-space features associated with different production mechanisms, providing detailed insights into the underlying reaction dynamics.

Furthermore, these processes may constitute a pathway for producing rare isotopes in complex nuclear systems. Overall, this work provides a consistent theoretical framework and quantitative predictions that can serve as a useful reference for future experimental investigations.

II. THEORETICAL FRAMEWORK

A. UrQMD model

The UrQMD model is a microscopic, many-body theoretical framework based on transport theory. In this model, nucleons are described as Gaussian wave packets with finite spatial widths, whose centroids in coordinate and momentum space evolve dynamically under the system Hamiltonian [35, 36]. The Hamiltonian incorporates several terms, including two- and three-body Skyrme interactions, Yukawa potentials, Coulomb interactions, Pauli blocking, symmetry energy contributions, and momentum-dependent potentials. Detailed parameters for these interactions are provided in Ref. [35]. These terms collectively govern the interactions among nucleons and determine their spatiotemporal evolution through the Hamiltonian equations of motion:

$$\frac{\mathrm{d}\boldsymbol{r}_i}{\mathrm{d}t} = \frac{\partial H}{\partial \boldsymbol{p}_i}, \tag{1}$$

$$\frac{\mathrm{d}\boldsymbol{p}_i}{\mathrm{d}t} = -\frac{\partial H}{\partial \boldsymbol{r}_i}, \tag{2}$$

where $\boldsymbol{r}_i$ and $\boldsymbol{p}_i$ denote the position and momentum of the ith nucleon, respectively. Additionally, the UrQMD model incorporates stochastic processes such as particle scattering and decay, which are modeled using experimentally measured cross sections and resonance parameters. Therefore, the UrQMD model provides a comprehensive description of various physical mechanisms in nuclear reactions over a broad energy range, including elastic and inelastic scattering, resonance excitation and decay, and meson production. Consequently, the model reproduces experimentally observed particle production probabilities, rapidity distributions, and angular distributions with reasonable accuracy [35−37].

To date, the UrQMD model has been extensively applied to simulate nuclear reactions over a wide energy range, from SIS to RHIC. These applications include nucleon–nucleus collisions [38], nucleus–nucleus collisions [39−42], and strange particle production [38, 43]. Previous studies have shown that the UrQMD model is suitable for investigating heavy-ion collisions in the medium-energy regime. In this paper, the UrQMD model is employed to simulate and analyze CE reactions accompanied by single-π^+ production in medium-energy heavy-ion collisions.

The numerical simulations in this study are performed using the UrQMD model. To ensure reproducibility and account for model sensitivity in the medium-energy regime, we specify the detailed settings as follows. We simulate ^{12}C + ^{12}C collisions at incident energies of 400, 500, and 600 A MeV. All calculations are conducted in the laboratory reference frame. The impact parameter is set to $b = 0$–5.5 fm, covering central to peripheral collisions. Because single-π^+ CE reactions require sufficient nuclear overlap for Δ resonance production, this range encompasses most of the relevant events for the

$^{12}C+{}^{12}C$ system.

A hard Skyrme-type EoS is adopted for the nuclear mean-field potential, which is suitable for describing the collective dynamics and pion production in this energy regime. The initial nuclei are prepared using a stabilization procedure consistent with the quantum molecular dynamics (QMD) mean-field, instead of a simple Woods–Saxon initialization. This treatment ensures the structural stability and proper binding energies of the projectile and target, avoiding unphysical pre-collision oscillations and nucleon emission.

The dynamical evolution is followed up to a total propagation time of 100 fm/c. By this time, the system reaches the low-density freeze-out stage, where fragment formation and pion production have stabilized and yields have saturated [44].

B. Phase-space coalescence model

The phase-space coalescence model is applied to the final-state nucleons from the UrQMD simulations to reconstruct and identify the nuclear fragments produced in the reaction. This model has been widely used in dynamical models, including the Boltzmann–Uehling–Uhlenbeck (BUU), QMD, and UrQMD frameworks, to identify nuclear clusters and estimate their yields [45–47]. It has been shown to provide a reliable description of cluster formation in the medium-energy regime for nuclei with mass numbers $A=1$–14 [48]. Thus, it is well-suited for describing fragment formation in the $A=12$ reaction system considered in this paper.

In the final state of the collision, emitted nucleons that are sufficiently close in phase space are assumed to originate from the same primary fragment and are thus considered to form a cluster. In this model, two nucleons i and j are considered to belong to the same cluster if the following conditions are satisfied:

$$|\boldsymbol{p}_i-\boldsymbol{p}_j|<p_0,\quad |\boldsymbol{r}_i-\boldsymbol{r}_j|<r_0, \tag{3}$$

where p_0 and r_0 denote the momentum- and coordinate-space coalescence parameters, respectively. Typically, p_0 and r_0 range from 0.25 to 0.35 GeV/c and from 3 to 4 fm, respectively [46].

To examine the sensitivity of the coalescence production probabilities to p_0 and r_0, we perform simulations with 10^6 events at an incident energy of 500 A MeV. The production probabilities of ^{12}N and ^{12}Be are evaluated for different parameter sets, as shown in Figs. 1 and 2. The error bars represent the square root of the number of events ($\sqrt{N}$), corresponding to Poisson statistical uncertainties. The results indicate that the production probabilities are weakly dependent on p_0 but increase significantly with r_0.

This behavior can be understood in terms of the underlying reaction mechanism. Given that the projectile, target, and fragments share the same mass number ($A=12$), the reaction is dominated by peripheral collisions. In such collisions, nucleons experience minimal deflection and remain spatially localized, resulting in a strong dependence of the production probability on the coordinate-space criterion r_0. In contrast, the small momentum transfer limits the variation in relative momenta among nucleons participating in the coalescence process. Consequently, varying the momentum-space criterion p_0 has a minimal effect on the number of nucleons satisfying the coalescence condition, leading to a weak dependence of the production probability on p_0.

Because the phase-space coalescence model is fundamentally a phenomenological tool intended for order-of-magnitude estimations and trend analysis, its parameters can assume a reasonable range of values. Considering the distinct interactions between nucleon pairs, particularly the Coulomb repulsion between protons, a smaller coales-

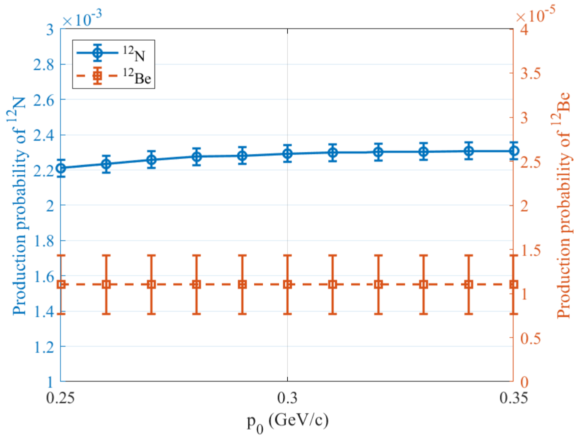

Fig. 1. (color online) Effect of p_0 on the production probabilities of ^{12}N and ^{12}Be in $^{12}C+{}^{12}C$ collisions at 500 A MeV ($r_0=3.8$ fm).

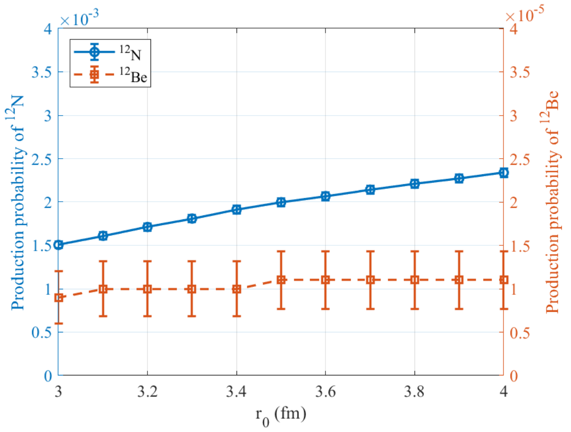

Fig. 2. (color online) Effect of r_0 on the production probabilities of ^{12}N and ^{12}Be in $^{12}C+{}^{12}C$ collisions at 500 A MeV ($p_0=0.25$ GeV/c).

cence radius is adopted for proton–proton pairs. In this study, we adopt the momentum-space coalescence parameter and coordinate-space coalescence radii as

$$p_0 = 0.25\ \text{GeV}/c, \quad r_{pp} = 2.8\ \text{fm}, \quad r_{nn} = r_{np} = 3.8\ \text{fm}. \quad (4)$$

The momentum of a reconstructed fragment is calculated by summing the momenta of its constituent nucleons:

$$\boldsymbol{p} = \sum_i \boldsymbol{p}_i = (\boldsymbol{p}_x, \boldsymbol{p}_y, \boldsymbol{p}_z), \quad (5)$$

and the magnitude of the total momentum is given by

$$p = \sqrt{\boldsymbol{p}_x^2 + \boldsymbol{p}_y^2 + \boldsymbol{p}_z^2}. \quad (6)$$

The total energy is then calculated using the relativistic energy–momentum relation:

$$E = \sqrt{p^2c^2 + m^2c^4}, \quad (7)$$

where m is the rest mass of the fragment. This simple and efficient method is widely used in transport-model analyses of nuclei production in medium- to high-energy heavy-ion collisions.

In this paper, we focus on the reaction channel ^{12}C(^{12}C, ^{12}Nπ^+)^{12}Be to investigate CE reactions accompanied by the production of a single π^+ meson. This channel is particularly advantageous because ^{12}N possesses no bound excited states and exists only in its ground state [49], thereby eliminating uncertainties associated with excitation energies. Consequently, the total energies of ^{12}N and π^+ can be accurately determined using their rest masses, $m(^{12}\text{N}) = 12.0186132\ \text{u} \approx 11.195\ \text{GeV}$ and $m(\pi^+) \approx 0.139\ \text{GeV}$ [50, 51]. The nucleon dynamics at incident energies of 400,500, and 600 A MeV are simulated using the UrQMD model, after which the coalescence model is applied to reconstruct the final-state fragments.

III. RESULTS

In this paper, we employ the UrQMD model to simulate 1.44×10^9 events for the $^{12}\text{C}+^{12}\text{C}$ incident channel at medium energies (400, 500, and 600 A MeV). The final-state nucleons from the collisions are subsequently analyzed using a phase-space coalescence model to calculate the event production probability for the specific reaction channel: ^{12}C(^{12}C, ^{12}Nπ^+)^{12}Be.

The reaction cross section at each incident energy is calculated as described in [32]:

$$\sigma = A_{\text{reaction}} \cdot \frac{N}{N_{\text{total}}}, \quad (8)$$

where σ denotes the cross section for the channel of interest, A_{reaction} represents the geometric reaction area, N_{total} is the total number of simulated events, and N is the number of events corresponding to the selected reaction channel. In the simulation, the impact parameter b is sampled according to the geometric prescription.

$$\mathrm{d}\sigma = 2\pi b\,\mathrm{d}b, \quad (9)$$

yielding a probability distribution:

$$\frac{\mathrm{d}P}{\mathrm{d}b} \propto b. \quad (10)$$

Sampling is performed over the range $0 \le b \le 5.5$ fm, yielding $A_{\text{reaction}} = \pi\times(5.5\,\text{fm})^2$.

For the ^{12}C(^{12}C,^{12}Nπ^+)^{12}Be reaction, the numbers of identified events are 13, 24, and 30, yielding cross sections of 8.58 ± 2.38 nb, 15.84 ± 3.23 nb, and 19.80 ± 3.61 nb, respectively. As shown in Fig. 3, the cross section increases monotonically with the incident energy.

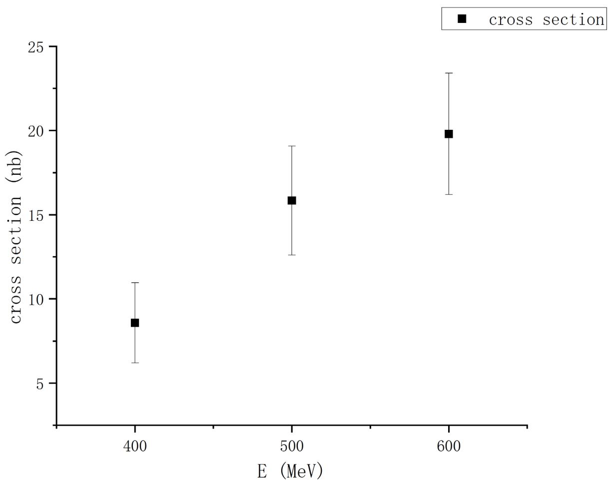

Fig. 3. Cross sections for the ^{12}C(^{12}C, ^{12}Nπ^+)^{12}Be reaction at 400, 500, and 600 A MeV.

We further investigate the dynamical properties of the ^{12}C(^{12}C,^{12}Nπ^+)^{12}Be reaction. By analyzing the energy and momentum distributions, along with other relevant observables of the reaction products, we aim to elucidate the underlying reaction dynamics and identify characteristic phase-space features associated with different production mechanisms. Additionally, we explore potential pathways for rare isotope production and provide quantitative predictions to guide future experimental studies.

A. Momentum and energy distributions for the ^{12}C(^{12}C, ^{12}Nπ^+)^{12}Be reaction

In this subsection, we examine the momentum and energy distributions of the emitted ^{12}N nuclei and π^+ mesons in the laboratory frame. This analysis provides direct insight into the kinematic characteristics of the reaction products and illuminates the underlying mechanisms of energy and momentum transfer during the collision. To achieve a comprehensive understanding, we systematically investigate the total, longitudinal, and transverse momentum distributions, along with the corresponding energy distributions.

The total momentum distributions of the emitted ^{12}N nuclei in the laboratory frame are presented in Fig. 4. Owing to limited statistics in several datasets, statistical uncertainties are evaluated using exact Poisson confidence intervals (Garwood method) rather than the $\sqrt{N}$ approximation [52]. These confidence intervals are derived from the chi-squared distribution and correspond to a 95% confidence level ($\alpha = 0.05$).

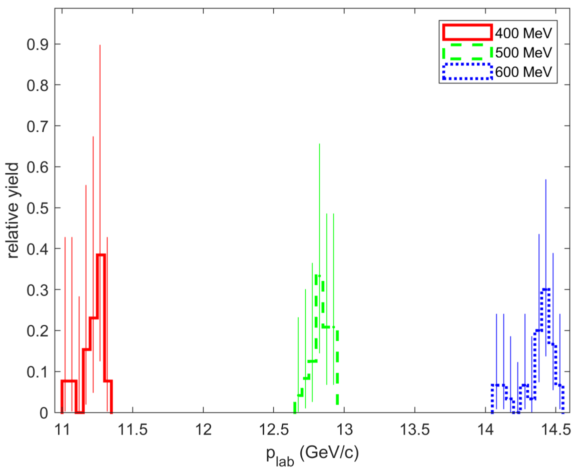

Fig. 4. (color online)Normalized total momentum distributions of emitted ^{12}N nuclei in the laboratory frame for the ^{12}C(^{12}C, ^{12}Nπ^+)^{12}Be reaction at incident energies of 400, 500, and 600 A MeV.

Under this statistical treatment, the extracted distributions exhibit a clear systematic trend. As the incident energy increases from 400 to 600 A MeV, the peak position shifts toward higher momentum, accompanied by a decrease in peak height, whereas the overall width remains essentially unchanged.

The longitudinal momentum distributions in the laboratory frame are presented in Fig. 5. The normalized p_L distributions exhibit features similar to those of the total momentum distributions. In particular, as the incident energy increases, the peak position shifts toward higher momentum, accompanied by a decrease in peak height, whereas the distribution width remains essentially unchanged.

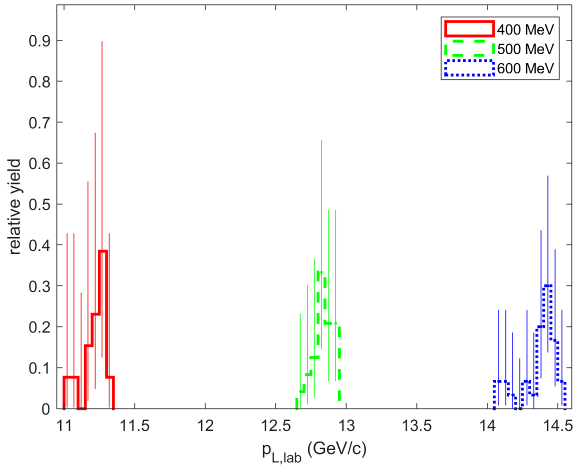

Fig. 5. (color online) Normalized longitudinal momentum distributions of the emitted ^{12}N nuclei in the laboratory frame for the reaction ^{12}C(^{12}C, ^{12}Nπ^+)^{12}Be at incident energies of 400, 500, and 600 A MeV.

The transverse momentum distributions are presented in Fig. 6. In contrast to the longitudinal distributions, the normalized p_T distributions exhibit nearly identical shapes across all three incident energies. The distributions display pronounced maxima in the low-p_T region, with the dominant contributions concentrated within $p_{T,\rm lab} \approx 0.05$–$0.25$ GeV/c. Within the uncertainties, no significant shift in the peak position or notable change in width is observed as the incident energy increases, indicating a weak dependence of the transverse momentum on incident energy.

The energy distributions of the emitted ^{12}N nuclei are

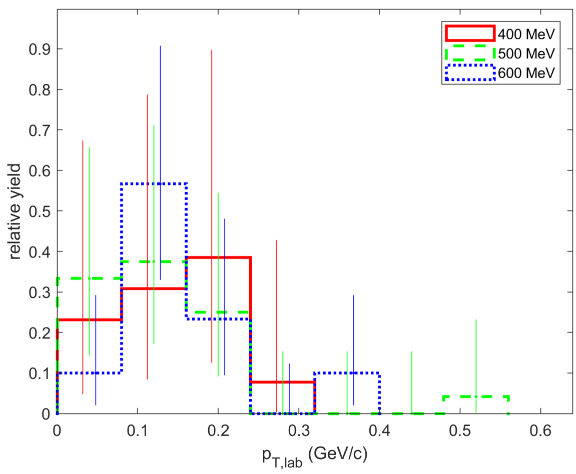

Fig. 6. (color online) Normalized transverse momentum distributions of the emitted ^{12}N nuclei in the laboratory frame for the reaction ^{12}C(^{12}C, ^{12}Nπ^+)^{12}Be at incident energies of 400, 500, and 600 A MeV.

presented in Fig. 7. As the incident energy increases from 400 to 600 A MeV, the peak position shifts toward higher energies, whereas the overall width remains essentially constant and the peak height decreases slightly.

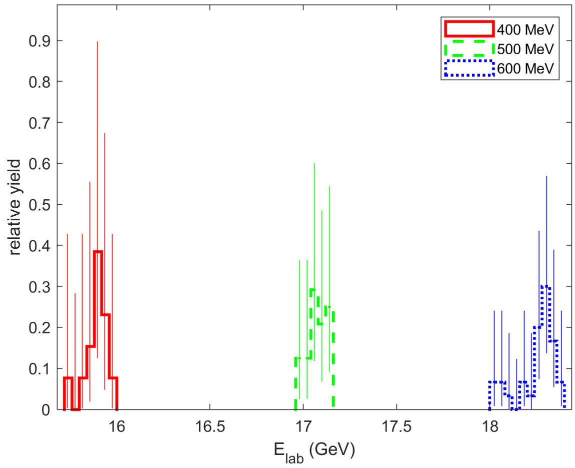

Fig. 7. (color online) Normalized laboratory-frame energy distributions of emitted ^{12}N nuclei for the reaction ^{12}C(^{12}C, ^{12}Nπ^+)^{12}Be at incident energies of 400, 500, and 600 A MeV.

In summary, a coherent picture emerges from the momentum and energy distributions. The incident energy primarily influences the longitudinal dynamics of the emitted fragments, as reflected by systematic shifts in the total and longitudinal momentum distributions, whereas the transverse momentum distributions remain largely unchanged. The approximately constant widths suggest that the fragmentation process predominantly preserves the intrinsic momentum spread of the projectile. These characteristics indicate that ^{12}N production is dominated by peripheral collisions, in which the projectile undergoes limited energy dissipation, rather than by central collisions associated with substantial momentum and energy transfer.

Subsequently, we analyze the total, longitudinal, and transverse momentum distributions, as well as the energy distribution, of the emitted π^+ mesons in the laboratory frame to elucidate their production mechanism in the ^{12}C(^{12}C, ^{12}Nπ^+)^{12}Be reaction. These distributions characterize the kinematic behavior of the π^+ mesons and provide insights into the underlying reaction dynamics.

As shown in Figs. 8, 9, and 10, the produced π^+ mesons exhibit low total, longitudinal, and transverse momenta, with minimal variation as the incident energy increases. The similarity between the longitudinal and transverse distributions indicates that the motion of the π^+ mesons is nearly isotropic. The energy distributions, shown in Fig. 11, exhibit a similarly weak dependence on the incident energy, consistent with the trends observed in

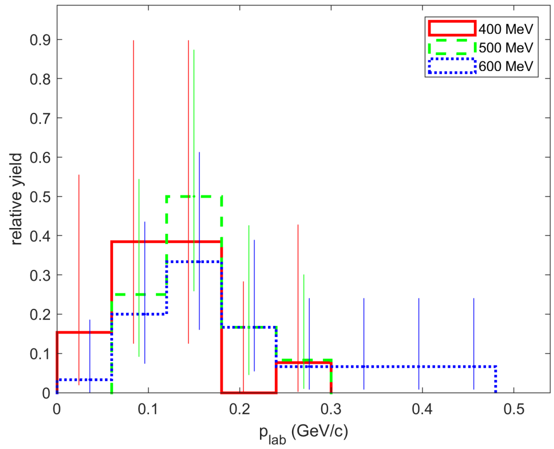

Fig. 8. (color online) Normalized total momentum distributions, in the laboratory frame, of π^+ mesons produced in the reaction ^{12}C(^{12}C, ^{12}Nπ^+)^{12}Be at incident energies of 400, 500, and 600 A MeV.

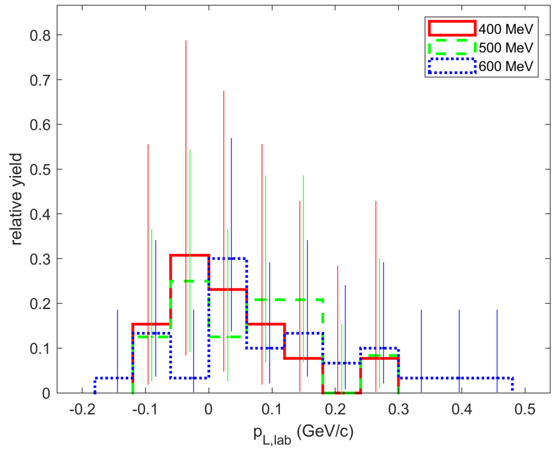

Fig. 9. (color online) Normalized longitudinal momentum distributions of produced π^+ mesons in the laboratory frame for the reaction ^{12}C(^{12}C, ^{12}Nπ^+)^{12}Be at incident energies of 400, 500, and 600 A MeV.

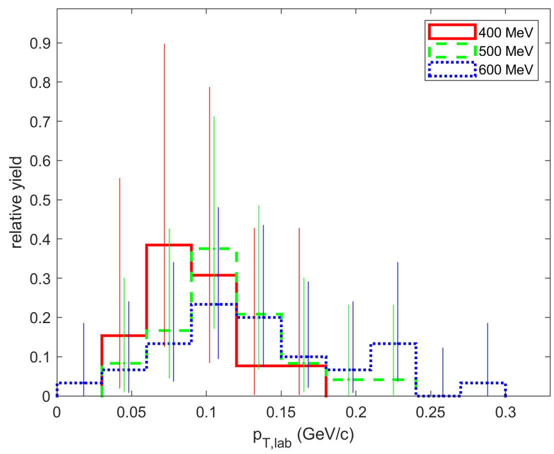

Fig. 10. (color online) Normalized transverse momentum distributions of produced π^+ mesons in the laboratory frame for the reaction ^{12}C(^{12}C, ^{12}Nπ^+)^{12}Be at incident energies of 400, 500, and 600 A MeV.

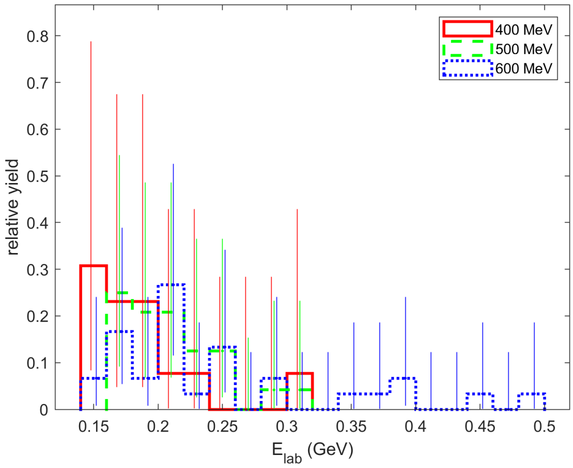

Fig. 11. (color online) Normalized energy distributions of π^+ mesons in the laboratory frame for the reaction $^{12}C(^{12}C, ^{12}N\pi^+)^{12}Be$ at incident energies of 400, 500, and 600 *A* MeV.

the momentum distributions.

These characteristics are inconsistent with direct reaction processes, which typically yield high-momentum, forward-peaked pions. They are also inconsistent with the decay of the emitted ^{12}N nucleus. Because the ^{12}N nucleus carries a large longitudinal momentum, its decay products would be strongly forward-peaked in the laboratory frame. Instead, the observed low-momentum, quasi-isotropic distributions suggest that the π^+ mesons are predominantly produced via the decay of Δ resonances. This scenario naturally explains both the weak energy dependence and the near isotropy of the momentum and energy distributions.

B. Angular Ddistributions for the $^{12}C(^{12}C, ^{12}N\pi^+)^{12}Be$ reaction

The emission angle θ is defined as the angle between the momentum vector of an emitted particle and the incident beam direction. It serves as a key observable for characterizing the spatial correlation between particle emission and the beam direction, and provides important guidance for the optimal placement of detectors in subsequent experiments.

In this work, the emission angles of the ^{12}N nuclei and π^+ mesons in the $^{12}C(^{12}C, ^{12}N\pi^+)^{12}Be$ reaction are calculated as!

$$\theta = \arctan\left(\frac{|\boldsymbol{p}_T|}{|\boldsymbol{p}_L|}\right), \tag{11}$$

where $|\boldsymbol{p}L|$ and $|\boldsymbol{p}T|$ denote the longitudinal and transverse momentum components with respect to the incident beam, respectively.

In the laboratory frame, the emitted ^{12}N nuclei are concentrated predominantly at small forward angles (0°–2.5°), as shown in Fig. 12. This pronounced forward peaking indicates that the momentum transfer from the incident ^{12}C nucleus occurs primarily along the beam direction, with negligible transverse components. Such a distribution is characteristic of peripheral single-CE reactions. Furthermore, the distribution shifts toward even smaller angles as the incident energy increases, suggesting that the ^{12}N emission becomes increasingly collimated along the beam axis at higher energies. These observations are consistent with the conclusion that ^{12}N is produced predominantly in peripheral collisions involving small momentum transfers.

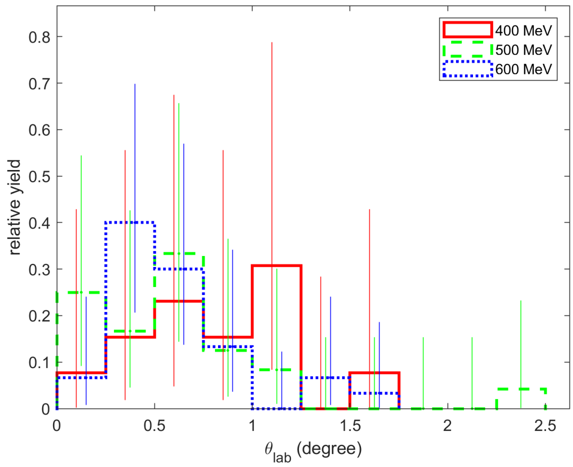

Fig. 12. (color online) Normalized angular distributions of emitted ^{12}N nuclei in the laboratory frame for the reaction $^{12}C(^{12}C, ^{12}N\pi^+)^{12}Be$ at incident energies of 400, 500, and 600 *A* MeV.

In contrast, the angular distributions of the π^+ mesons are much broader. In the laboratory frame, they extend from 0° to approximately 150°, as shown in Fig. 13(a), whereas the ^{12}N nuclei remain strongly forward-peaked. If the π^+ mesons were produced in the same direct reaction, their angular distributions would be expected to exhibit similar forward peaking. However, the observed broad distributions suggest a distinct production mechanism.

In the center-of-mass frame, the π^+ angular distributions remain broad, spanning approximately 5° to 165° as shown in Fig. 13(b). The majority of mesons are emitted at angles greater than 90°, exhibiting a pronounced backward enhancement. This backward peaking weakens with increasing incident energy. Such features are consistent with a multi-step reaction scenario, as suggested by the momentum and energy distributions. In this scenario, the incident nucleus first interacts with target nucleons to form an intermediate excited state, such as a Δ resonance,

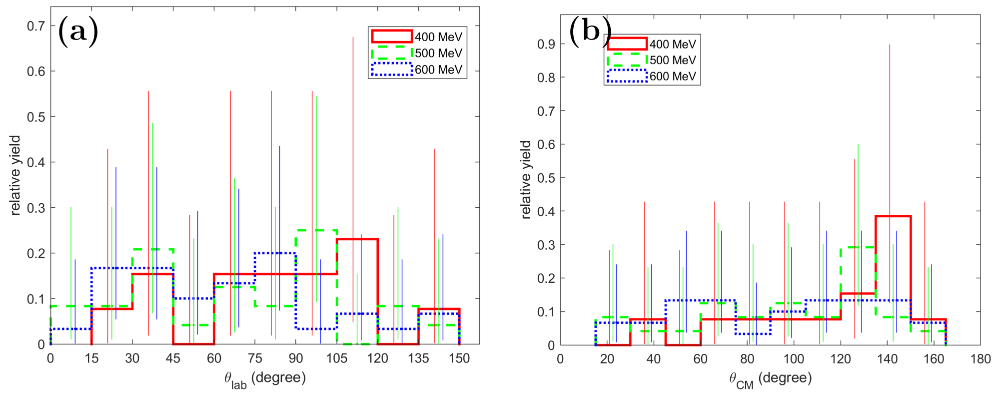

Fig. 13. (color online) (a) Normalized angular distributions of produced π^+ mesons in the laboratory frame for the reaction $^{12}C(^{12}C,\, ^{12}N\pi^+)^{12}Be$ at incident energies of 400, 500, and 600 AMeV. (b) Normalized angular distributions of produced π^+ mesons in the center-of-mass frame for the reaction $^{12}C(^{12}C,\, ^{12}N\pi^+)^{12}Be$ at incident energies of 400, 500, and 600 AMeV.

which subsequently decays into a π^+ meson. The redistribution of momentum among nucleons during this process naturally yields the observed broad and backward-enhanced angular distributions.

C. Rapidity distributions for the $^{12}C(^{12}C,\, ^{12}N\pi^+)^{12}Be$ reaction

While the angular distributions primarily reflect the emission geometry of the reaction products, rapidity provides complementary insight into their longitudinal dynamics. Therefore, we analyze the rapidity distributions of the emitted ^{12}N nuclei and π^+ mesons. Rapidity is defined as

$$y = \frac{1}{2}\ln\frac{E+|\boldsymbol{p}_L|}{E-|\boldsymbol{p}_L|}, \tag{12}$$

where E and p_L denote the total energy and longitudinal momentum of the particle, respectively. Because rapidity differences are invariant under longitudinal Lorentz boosts, rapidity provides a convenient, nearly frame-independent measure of longitudinal dynamics. Consequently, it serves as a sensitive probe of particle emission along the beam axis.

As shown in Fig. 14(a), the rapidity of the emitted ^{12}N nuclei increases with the incident beam energy. In contrast to central collisions, where particle production is concentrated around mid-rapidity, Fig. 14(b) shows that the rapidity distributions of the emitted ^{12}N nuclei peak in the high-rapidity region, close to the rapidity of the incident nucleus. Moreover, the rapidities of the emitted ^{12}N nuclei are at most 0.03 lower than the rapidity of the incident ^{12}C nucleus. This indicates that the formation of ^{12}N is dominated by the projectile, and that the participating nucleons undergo negligible thermalization or momentum exchange, consistent with the characteristics of peripheral collisions.

As shown in Fig. 15, the rapidity distributions of the π^+ mesons peak around $y \approx 0$, indicating that their longitudinal momenta are relatively small in the center-of-mass frame. A slightly higher yield is observed at negative rapidities. As the incident energy increases, the distribution shifts slightly toward positive rapidities, consistent with the weakening of the backward-emission feature observed in the angular distributions. The concentration at mid-rapidity suggests that these π^+ mesons originate predominantly from the participant region rather than from projectile-like fragments. This behavior aligns with the broad, backward-enhanced angular distributions and further supports the interpretation—drawn from momentum, energy, and angular analyses—that the π^+ mesons are predominantly produced via the decay of intermediate Δ resonances.

Overall, the rapidity distributions provide a complementary view of the angular emission patterns. The ^{12}N nuclei exhibit rapidities close to those of the incident nucleus, reflecting their projectile-dominated origin and the peripheral character of the reaction. In contrast, the π^+ mesons are concentrated at mid-rapidity, corresponding to small longitudinal momenta and consistent with their tendency toward backward emission in the center-of-mass frame. These features agree with the conclusions drawn from the momentum, energy, and angular analyses, providing a coherent picture in which the π^+ mesons are predominantly produced via the decay of intermediate Δ resonances in a multi-step process.

IV. DISCUSSION

In transport models such as UrQMD, CE-like effects may arise from various microscopic mechanisms, including genuine nucleon–nucleon CE reactions and effective CE processes, such as Δ resonance excitation followed by reabsorption and large-angle elastic nucleon–nucleon scattering. In a nuclear medium, these processes are further modified by Pauli blocking and density-dependent effects, complicating the unambiguous identification of

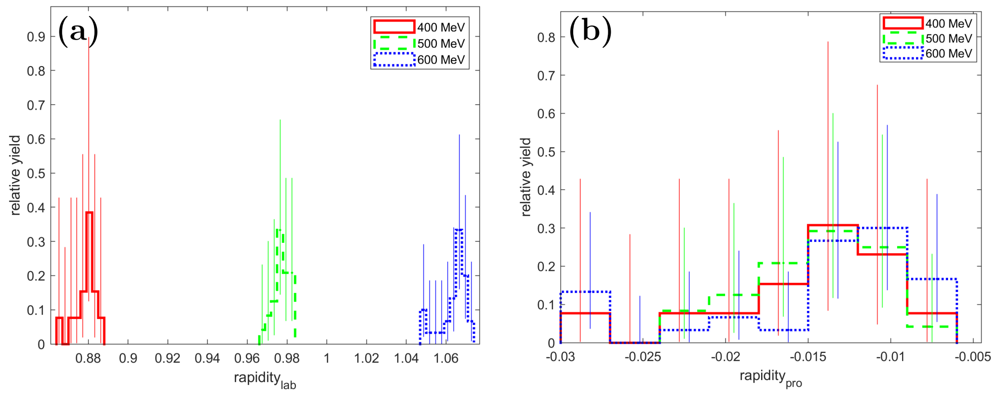

Fig. 14. (color online) (a) Normalized rapidity distributions of the emitted ^{12}N nuclei in the laboratory frame for the ^{12}C(^{12}C, ^{12}Nπ^+)^{12}Be reaction at incident energies of 400, 500, and 600 A MeV. (b) Normalized rapidity distributions of the emitted ^{12}N nuclei in the projectile frame for the ^{12}C(^{12}C, ^{12}Nπ^+)^{12}Be reaction at incident energies of 400, 500, and 600 A MeV.

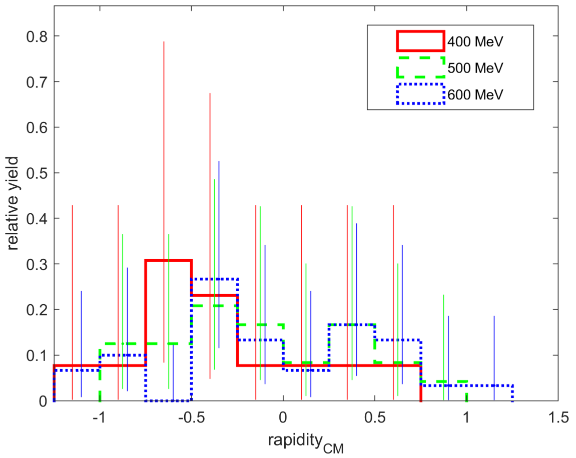

Fig. 15. (color online) Normalized center-of-mass rapidity distributions of π^+ mesons produced in the reaction ^{12}C(^{12}C, ^{12}Nπ^+)^{12}Be at incident energies of 400, 500, and 600 A MeV.

the underlying mechanisms.

The events analyzed in the present study,

$$^{12}\mathrm{C}+^{12}\mathrm{C}\rightarrow\, ^{12}\mathrm{Be}+\,^{12}\mathrm{N}+\pi^+,$$

correspond to peripheral collisions. In these events, only a few nucleon–nucleon collisions occur, and the associated momentum transfer is small, rendering large-angle elastic scattering highly improbable. Although multiple Δ excitations could, in principle, contribute, their probability at the present energies is negligible. Moreover, additional scatterings or excitations would result in greater nuclear excitation and reduce the likelihood that the residual nuclei remain bound [53]. Although a complete disentanglement of all mechanisms is not possible within the UrQMD model, the combined constraints from collision geometry, residue stability, and single π^+ emission favor a scenario dominated by a nucleon–nucleon CE reaction mediated by a single Δ excitation.

Furthermore, because the cross section for the ^{12}C(^{12}C,^{12}Nπ^+)^{12}Be reaction is much smaller than those of competing channels in ^{12}C+^{12}C collisions, a careful evaluation of the background is required to ensure that the selected events correspond to the channel of interest. Therefore, the missing–mass method is employed to reconstruct the unobserved system via energy–momentum conservation:

$$E_{\rm miss}=E_{\rm beam}+E_{\rm tgt}-E_{^{12}\rm N}-E_{\pi^+}, \tag{13}$$

$$\boldsymbol{P}_{\rm miss}=\boldsymbol{P}_{\rm beam}+\boldsymbol{P}_{\rm tgt}-\boldsymbol{P}_{^{12}\rm N}-\boldsymbol{P}_{\pi^+}, \tag{14}$$

$$M^2_{\rm miss}=E^2_{\rm miss}-|\boldsymbol{P}_{\rm miss}|^2. \tag{15}$$

Here, $E_{\rm miss}$, $\boldsymbol{P}_{\rm miss}$, and $M_{\rm miss}$ are the energy, momentum, and invariant mass of the unobserved system, respectively. The missing-mass distribution allows us to determine whether the reconstructed system corresponds to the expected residual nucleus, thereby serving as an effective tool for event selection in reactions with complex final states [54].

In practice, some emitted π^+ mesons may remain undetected, whereas other particles may be misidentified as π^+ mesons. These effects can lead to the misclassification of non-target channels as target events, thereby introducing background contributions. To quantify these effects, we analyze the multiplicity of π^+ mesons and the production of other mesons (such as π^0 and π^-) to identify potential background sources and estimate the maximum signal-to-background ratio.

Figure 16 shows the multiplicity distributions of π^+ mesons at 400, 500, and 600 A MeV when the residual projectile nucleus is ^{12}N and the heaviest target fragment has a mass number of $A = 12$. No events containing two

π^+ mesons are observed at any of the three energies. Furthermore, the numbers of events in which one π^+ meson is produced alongside other mesons are 0, 2, and 6 at 400, 500, and 600 A MeV, respectively.

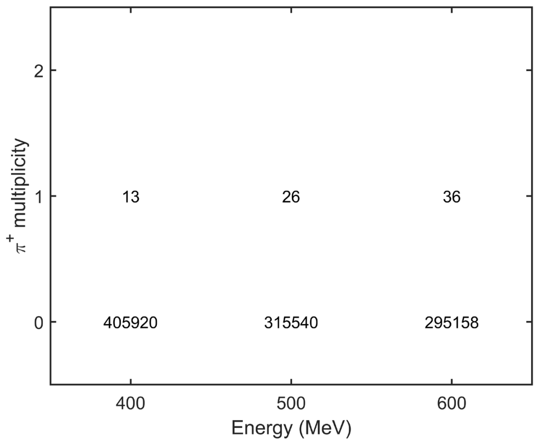

Fig. 16. Multiplicity distributions of π^+ in the $^{12}C+^{12}C$ reaction at incident energies of 400,500, and 600 A MeV for events in which the projectile residue is ^{12}N and the heaviest target fragment has a mass number of $A = 12$.

To estimate the signal-to-background ratio, we assume that the background follows a Poisson distribution. We adopt the 95% confidence-level upper limit for the number of background events, thereby providing a conservative estimate of the minimum signal-to-background ratio. The corresponding upper limits on the background are 3.00, 6.30, and 11.84 events at 400, 500, and 600 A MeV, respectively [55]. Consequently, the minimum signal-to-background ratios are approximately 4.33, 3.81, and 2.53, respectively.

In addition to background arising from detection inefficiencies, the residual target nucleus is unlikely to remain a single ^{12}Be nucleus; instead, it populates multi-fragment states such as $^{11}Be+n$ and $^{10}Be+n+n$, as shown in Figs. 17, 18, and 19. During missing-mass reconstruction, these channels introduce additional background, potentially compromising the purity and resolution of the spectra.

To estimate the impact of these channels on the target reaction, we employ the UrQMD model and consider a conservative worst-case scenario. Events in which the heaviest target fragment has a mass number of 11 are treated as

$$^{12}C+^{12}C\rightarrow^{12}N+\pi^{+}+^{11}Be+n,$$

and events with a heaviest fragment mass number of 10 as

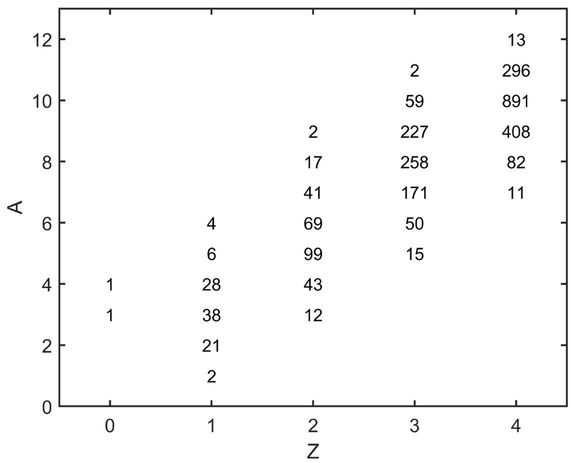

Fig. 17. Correlation between the mass number A and the charge Z of the heaviest target fragment produced in the $^{12}C(^{12}C, ^{12}N\pi^{+})$ reaction at an incident energy of 400 A MeV.

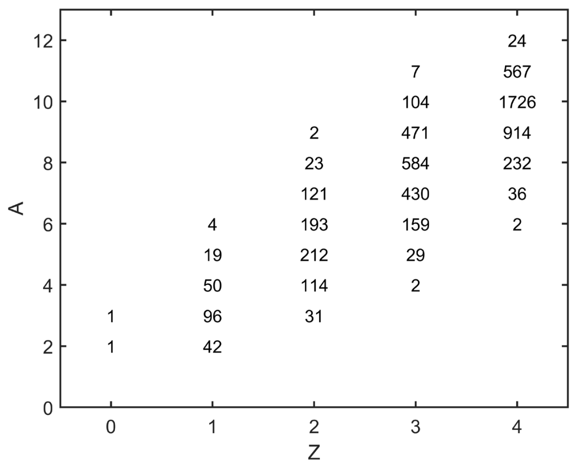

Fig. 18. Correlation between the mass number A and atomic number Z of the heaviest target fragment produced in the $^{12}C(^{12}C, ^{12}N\pi^{+})$ reaction at an incident energy of 500 A MeV.

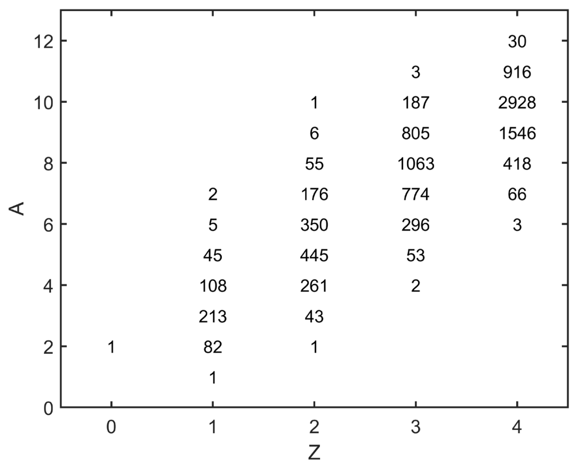

Fig. 19. Correlation between A and Z for the heaviest target fragment produced in the $^{12}C(^{12}C, ^{12}N\pi^{+})$ reaction at an incident energy of 600 A MeV.

$$^{12}\mathrm{C}+{}^{12}\mathrm{C}\rightarrow{}^{12}\mathrm{N}+\pi^{+}+{}^{10}\mathrm{Be}+n+n.$$

Under this assumption, at 400, 500, and 600 A MeV, the count ratios of the target channel

$$^{12}\mathrm{C}+{}^{12}\mathrm{C}\rightarrow{}^{12}\mathrm{N}+\pi^{+}+{}^{12}\mathrm{Be},$$

to the $^{11}\mathrm{Be}+n$ channels are 4.36×10^{-2}, 4.18×10^{-2}, and 3.37×10^{-2}, respectively; the corresponding ratios to the $^{10}\mathrm{Be}+n+n$ channels are 1.37×10^{-2}, 1.31×10^{-2}, and 9.63×10^{-3}.

V. CONCLUSION

In summary, we have conducted a comprehensive theoretical investigation of the $^{12}\mathrm{C}(^{12}\mathrm{C},{}^{12}\mathrm{N}\pi^{+})^{12}\mathrm{Be}$ reaction using the UrQMD model combined with a phase-space coalescence approach.

This work presents a novel investigation of a nontrivial heavy-ion CE channel in which CE processes and Δ resonance excitation occur simultaneously. While these mechanisms have primarily been studied in lepton-induced or light-ion reactions, this study extends the analysis to a many-body heavy-ion environment within the UrQMD model. The reaction, featuring single π^+ emission with ^{12}N predominantly in its ground state, yields a well-defined final-state configuration suitable for studying the reaction dynamics involving both CE processes and Δ resonance excitation and decay.

Our kinematic analysis reveals that the momentum, energy, emission angle, and rapidity of ^{12}N are strongly correlated with those of the incident ^{12}C nucleus. These correlations indicate that the reaction is dominated by peripheral, low-excitation collisions. In contrast, the π^+ mesons exhibit relatively low momentum and energy, broad angular and rapidity distributions, and a tendency toward backward emission in the center-of-mass frame, consistent with their production via the decay of intermediate Δ resonances.

Overall, this study offers guidance for rare-isotope production and experimental design, including detector configuration, beam-energy selection, and event-identification strategies. Future work will incorporate experimental data to further constrain the model and improve our understanding of heavy-ion CE reactions and associated meson-production mechanisms.

ACKNOWLEDGEMENTS

The authors gratefully acknowledge the support of the Supercomputing Center of Lanzhou University.

References

[1] L. Shvedov, M. Colonna, M. Di Toro, Phys. Rev. C **81**(5), 054605 (2010)
[2] Z. You, K.-J. Wu, and F. Liu, Chin. Phys. C **34**, 1436 (2010)
[3] Y. Leifels, T. Blaich, T. W. Elze, *et al.* (FOPI Collaboration), Phys. Rev. Lett. **71**(7), 963 (1993)
[4] Y. Awaya, T. Kambara, Y. Kanai, Int. J. Mass Spectrom. **192**(1), 49 (1999)
[5] M.-Q. Ding, D.-Q. Fang, and Y.-G. Ma, Nucl. Sci. Tech. **35**, 211 (2024)
[6] Y. H. Zhang, P. Zhang, X. H. Zhou *et al.*, Phys. Rev. C **98**, 014319 (2018)
[7] G. S. Li, J. Su, B. H. Sun *et al.*, Phys. Rev. C **107**, 024609 (2023)
[8] J. Su, L. Zhu, and E. Xiao, Phys. Rev. C **105**, 024608 (2022)
[9] Y. Zhang, J. Tian, W. Cheng *et al.*, Phys. Rev. C **95**, 041602 (2017)
[10] L. P. Csernai, T. L. Trueman, and P. D. Bond, Phys. Today **48**(3), 95 (1995)
[11] J. Adams *et al.*, Nucl. Phys. A **757**(1), 102 (2005)
[12] C. Y. Wong, *Introduction to High-energy Heavy-ion Collisions. Teaneck*(New York: World Scientific Pub. Co., 1989)
[13] M. S. Abdallah, B. E. Aboona, J. Adam *et al.*, Nature **614**, 244 (2023)
[14] J. Chen, X. Dong, X. He *et al.*, Nucl. Sci. Tech **35**, 214 (2024)
[15] W. Ahner, R. Brockmann, E. Grosse *et al.*, Zeitschrift für Physik A Hadrons and Nuclei **341**, 123 (1991)
[16] D. Miskowiec, W. Ahner, R. Barth *et al.*, Phys. Rev.Letters **72**, 3650 (1994)
[17] G. C. Yong, J. L. Rodríguez-Sánchez, Y. Zhang *et al.*, Phys. Rev. C **111**, 054617 (2025)
[18] B. I. Abelev, M. M. Aggarwal, Z. Ahammed *et al.*, Science **328**, 58 (2010)
[19] N. Yao, A. Sorensen, V. Dexheimer *et al.*, Phys. Rev. C **109**, 065803 (2024)
[20] P. Russotto, M. Cozma, E. De Filippo *et al.*, La Rivista del Nuovo Cimento **46**(1), 70 (2023)
[21] G. Q. Li, C. H. Lee, G. E. Brown, Nucl. Phys. **625**, 372 (1997)
[22] B. E. Aboona, J. Adam, J. R. Adams *et al.*, Phys. Rev. Lett. **130**, 212301 (2023)
[23] H. Feshbach, E. M. Henley, Phys. Today **45**(12), 84 (1992)
[24] H. Lenske, H. H. Wolter, H. G. Bohlen, Phys. Rev. Lett. **62**(13), 1457 (1989)
[25] H. Lenske, F. Cappuzzello, M. Cavallaro *et al.*, Prog. Part. Nucl. Phys. **109**, 103716 (2019)
[26] E.-W. Grewe, D. Frekers, S. Rakers *et al.*, Phys. Rev.C **76**(5), 054307 (2007)
[27] F. Cappuzzello, H. Lenske, M. Cavallaro *et al.*, Prog. Part. Nucl. Phys. **128**, 103999 (2023)
[28] T. Kohmura, Prog. Theor. Exp. Phys. **33**(3), 480 (1965)
[29] C. A. Mosbacher, F. Osterfeld, Phys. Rev. C **56**(4), 2014 (1997)
[30] F. Osterfeld, Rev. Mod. Phys. **64**(2), 491 (1992)
[31] E. Bleszynski, M. Bleszynski, R. J. Glauber, Phys. Rev.

Lett. **60**(15), 1483 (1988)
[32] T. R. Saito, H. Ekawa, M. Nakagawa, Eur. Phys. J. A **57**(5), 159 (2021)
[33] T. R. Saito, W. Dou, V. Drozd *et al*., Nat. Rev. Phys. **3**(12), 803 (2021)
[34] T. Shao, J. Chen, J. Pochodzalla *et al*., Phys. Rev. Lett. **134**(16), 162501 (2025)
[35] S. A. Bass, M. Belkacem, M. Bleicher *et al*., Prog. Part. Nucl. Phys. **41**, 255 (1998)
[36] M. Bleicher, E. Bratkovskaya, Prog. Part. Nucl. Phys. **122**, 103920 (2022)
[37] M. Bleicher, E. Zabrodin, C. Spieles *et al*., J. Phys. G **25**(9), 1859 (1999)
[38] A. Limphirat, C. Kobdaj, M. Bleicher *et al*., J. Phys. G **36**(6), 064049 (2009)
[39] P. Russotto, S. Gannon, S. Kupny *et al*., Phys. Rev.C **94**(3), 034608 (2016)
[40] J. Thakur, A. Mukhopadhyay, P. Mali, Nucl. Phys. **1035**, 122659 (2023)
[41] Y. Wang, C. Guo, Q. Li *et al*., Phys. Rev. C **89**, 034606 (2014)
[42] F. Li, Y. Wang, Z. Gao *et al*., Phys. Rev. C **104**, 034608 (2021)
[43] G. Graef, J. Steinheimer, F. Li *et al*., Phys. Rev. C **90**(6), 064909 (2014)
[44] Q. Li, Z. Li, S. Soff *et al*., J. Phys. G **31**(11), 1359 (2005)
[45] S. Sombun, K. Tomuang, A. Limphirat *et al*., Phys. Rev. C **99**(1), 014901 (2019)
[46] Q. Li, Y. Wang, X. Wang *et al*., Sci. China-Phys. Mech. Astron. **59**(7), 672013 (2016)
[47] J. L. Nagle, B. S. Kumar, D. Kusnezov *et al*., Phys. Rev. C **53**(1), 367 (1996)
[48] H. Kruse, B. V. Jacak, J. J. Molitoris *et al*., Phys. Rev. C **31**, 1770 (1985)
[49] F. G. Kondev, M. Wang, W. J. Huang *et al*., Chin. Phys. C **45**(3), 030001 (2021)
[50] M. Wang, W. J. Huang, F. G. Kondev *et al*., Chin. Phys. C **45**(3), 030003 (2021)
[51] S. Navas *et al*., Phys. Rev. D **110**, 030001 (2024)
[52] F. Garwood, Biometrika **28**(3/4), 437 (1936)
[53] J. P. Bondorf, A. S. Botvina, A. S. Iljinov *et al*., Phys. Rept. **257**, 133 (1995)
[54] S. Koyama, D. Suzuki, M. Assié *et al*., Nucl. Instrum. Methods Phys. Res. A **1010**, 165477 (2021)
[55] G. Cowan, *Statistical Data Analysis* (Oxford: Oxford University Press, 1998)